Fuel 296 (2021) 120693

Contents lists available at ScienceDirect

Fuel

journal homepage: www.elsevier.com/locate/fuel

Full Length Article

Catalytic oxidative desulphurization of pyrolytic oils to fuels over different waste derived carbon-based catalysts

Valentina Tamborrino [a], Giulia Costamagna [b], Mattia Bartoli [a,c,*], Massimo Rovere [a,c], Pravin Jagdale [d], Luca Lavagna [a,c], Marco Ginepro [b], Alberto Tagliaferro [a,c]

[a] Department of Applied Science and Technology, Polytechnic of Turin, C.so Duca degli Abruzzi 24, Turin 10129, Italy
[b] Department of Chemistry, University of Turin, Via Pietro Giuria, 5, Torino 10125, Italy
[c] National Consortium for Materials Science and Technology (INSTM), Via G. Giusti 9, Florence 50121, Italy
[d] Center for Sustainable Future, Italian Institute of Technology, Via Livorno 60, Turin 10144, Italy

A R T I C L E I N F O

Keywords:
Biochar
Drop-in fuel
Tires
Pyrolysis
Biphasic catalysis

A B S T R A C T

In this work, we reported the conversion though carbothermal process of two catalysts produced by pyrolyzing exhausted coffee and waste tires. We tailored the surface with anchored iron nanoparticles through a facile carbothermal route and tested them for catalytic oxidative desulphurization of high sulphur content oil derived from tires pyrolysis. We studied their activity in a biphasic system under different conditions reaching a desulphurization of up to of 60% by using an oil with a sulphur concentration of up to 7139 ppm. The extensive characterization proved the reliability of those materials as promising catalysts for upgrading of sulphur rich drop-in fuels.

1. Introduction

Increased accountability of European Union with regards to environmental issues has represented a formidable driving force for the development of sustainable processes [1]. As a consequence, tires landfilling was forbidden with the European Council Directive 1999/31/CE due to its dangerous impact on the environment and human health [2,3]. Furthermore, sustainable and circular economy principles have growth leading to the exploration of alternatives end-life tires processes [4].

The simpler methods are their use as inert filler for constructions [5,6] and as road asphalt [7] or for the direct production of raw materials such as rubber [8–10] and textiles [11]. Alternatively, thermochemical routes are cost-effective approaches for end-life tires treatment avoiding the complexity of alternative management routes [12] such their conversion through pyrolytic techniques [13,14].

Oil recovered from pyrolysis of tires is a very attractive product stream due to their composition that is very close to an engine fuel [15]. Nonetheless, their sulphur content is generally very high avoiding their for real field applications and requires an upgrading process to met the fuel regulation requires.

Among the all upgrading procedure, catalytic oxidative desulphurization [16] is very interesting for meeting the sulphur limits of common fuels [17] under the principles of green chemistry [18]. Plenty of different approached are described in literature based on transition metal-based catalysts (i.e. cobalt [19], tungsten [20] and manganese [21] or polyoxometalates [22]) using air [23,24] or peroxides as oxidant agents [25–27], in homogenous or biphasic systems [28–31].

Iron-based catalysts are very promising due to their low cost price and to the ability to enhance oxidative power of oxygenated water [32] through Fenton mechanism [33].

This procedure achieved remarkably performances in the degradation of benzothiophene [34] and desulphurization of diesel-like fuels [35] by using nanostructured catalysts. Nonetheless, these systems were produced by using unfriendly procedures and lead to the merely deposition of the iron nanoparticles onto the support surface. Carbothermal route could represent a simple and facile alternative to produce iron nanoparticles anchored onto carbon support through thermochemical conversion of iron salts to metal iron nanoparticles [36,37].

In this study, we exploited the synergist effect of the use of waste-derived carbon support for the upgrading of waste-derived drop-in fuel. The integration of waste valorization and alternative fuels production could represent a first step for a deep re-think of sustainable

* Corresponding author.
E-mail address: mattia.bartoli@polito.it (M. Bartoli).

https://doi.org/10.1016/j.fuel.2021.120693
Received 7 January 2021; Received in revised form 2 March 2021; Accepted 15 March 2021

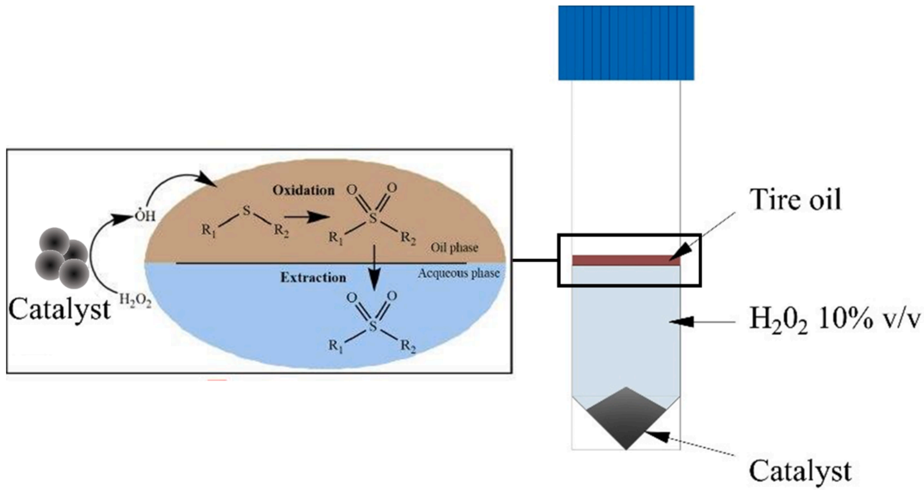

Fig. 1. Scheme of catalytic set-up.

platforms.

Here, we reported the development of two nanostructured iron-based catalysts produced though carbothermal conversion of exhausted coffee residues biochar (CC) and carbon recovered from the very same tire pyrolysis (TC). Nanostructured catalysts were used to upgraded oil from pyrolysis of tires though a biphasic catalytic desulphurization in a watery biphasic system.

The catalytic activity and catalyst structures were widely analyzed and compared achieving good results in desulphurization of high sulphur content oils. We also evaluated the effect of microstructured (CC) and nanostructured (TC) support in the catalytic performances.

2. Materials and methods

2.1. Materials

Fe $(NO_3)_3$ nonahydrate EtOH (>98%), HNO_3 (65%) and H_2O_2 (30% v/v) were purchased by Sigma Aldrich. Coffee powder was collected from Bar Katia (Turin, Italy) supplied by Vergnano (Arabica mixture). A Pirelli branched tire was used for this study.

2.2. Methods

2.2.1. Pyrolysis

Coffee was collected and dried at 105 °C prior the pyrolytic process. Afterwards, 100 g were pyrolyzed using a vertical furnace and a quartz reactor, heating rate of 15 °C/min and kept at 800 °C for 30 min accordingly with previous studies [38–41].

Tire was chopped in small pieces and pyrolized using a tubular furnace (Carbolite TZF 12/65/550) in nitrogen by using a heating rate of 15 °C/min and kept at 550 °C for 30 min. Solid and liquid fractions were collected.

A thermogravimetrical analysis (TGA) of the oil was performed from 25 to 900 °C using a TGA Mettler Toledo model 1600 in two different atmospheres (Argon and air) with a gas flux of 50 mL/min with a heating ramp of 10 °C/min to describe a possible oil composition.

2.2.2. Preparation and characterization of catalysts

Recovered carbon from tire and biochar produced by pyrolyzing exhausted coffee were used as starting materials for carbothermal process. 50 g of each of them were suspended in 250 mL of deionized water together with $Fe(NO_3)_3$ (weight of Fe/ weight carbon precursor of 1:10). The solution was stirred for 10 min and dried in a ventilated oven at 105 °C overnight. The dried materials were used without any additional purifications. Carbothermal process was run by using a tubular furnace (Carbolite TZF 12/65/550) in nitrogen atmosphere with a heating rate of 15 °C/min and kept at 800 °C for 30 min. The solids recovered were analyzed prior and after carbothermal processes by using several techniques.

Morphology was studied by using a field emission scanning electron microscope (FESEM, Zeis SupraTM40, Oberkochen, Germany). The microscope was equipped with an energy dispersive X-ray detector (EDX, Oxford Inca Energy 450, Oberkochen, Germany) that was used to explore the elemental composition of catalysts.

Raman spectra were collected by using Renishaw® Ramanscope InVia (H43662 model, Gloucestershire, UK). Signals were fitted according to methodology proposed by Tagliaferro et al. [42].

Surface of catalysts was investigated by using X-ray photoelectron spectroscopy (XPS). XPS spectrometer was a PHI 5000 Versaprobe Physical Electronics, Chanhassen, MN, USA) scanning X-ray photoelectron spectrometer (monochromatic Al K-alpha X-ray source with 1486.6 eV energy, 15 kV voltage, and 1 mA anode current) to investigate surface chemical composition.

Specific surface area of the samples was measured by means of N_2 sorption at −196 °C on a micrometrics Tristar II instrument (Micromeritics Instrument Corporation, USA). Brunauer–Emmett–Teller (BET) model was applied.

2.2.3. Catalysis

Catalytic tests were run in a biphasic systems as sketched in Fig. 1.

Catalysts were suspended in a 15 mL of a watery phase of H_2O_2 (10 v/v%) and 2 g of oil recovered from pyrolysis of tires were added. The sealed vials were put in an oil bath at different temperatures (60, 80 and 100 °C), for different time (2, 4 and 6 h) and by using several catalysts loading. After the reaction, they were cooled down at room temperature and 10 mL of deionized water were added. Oily phases were collected and purified by suspended particles by using a centrifuge (1000 rpm for 10 min). Recovered catalysts were collected, washed with acetone, dried at 105 °C overnight and further analyzed.

Sulphur concentration was determined by ICP (ICP-OES Perkin Elmer Optima 2000 DV) after acidic digestion in microwave oven (ETHOSUP Milestone) by using H_2O_2 30 v/v% in HNO_3 65 wt% (ratio 1:9) with a power of 800 W for 35 min.

3. Results and discussion

3.1. Characterization of the catalysts

Solid recovered from pyrolytic conversion of both exhausted coffee powder and waste tires were used as starting materials for carbothermal

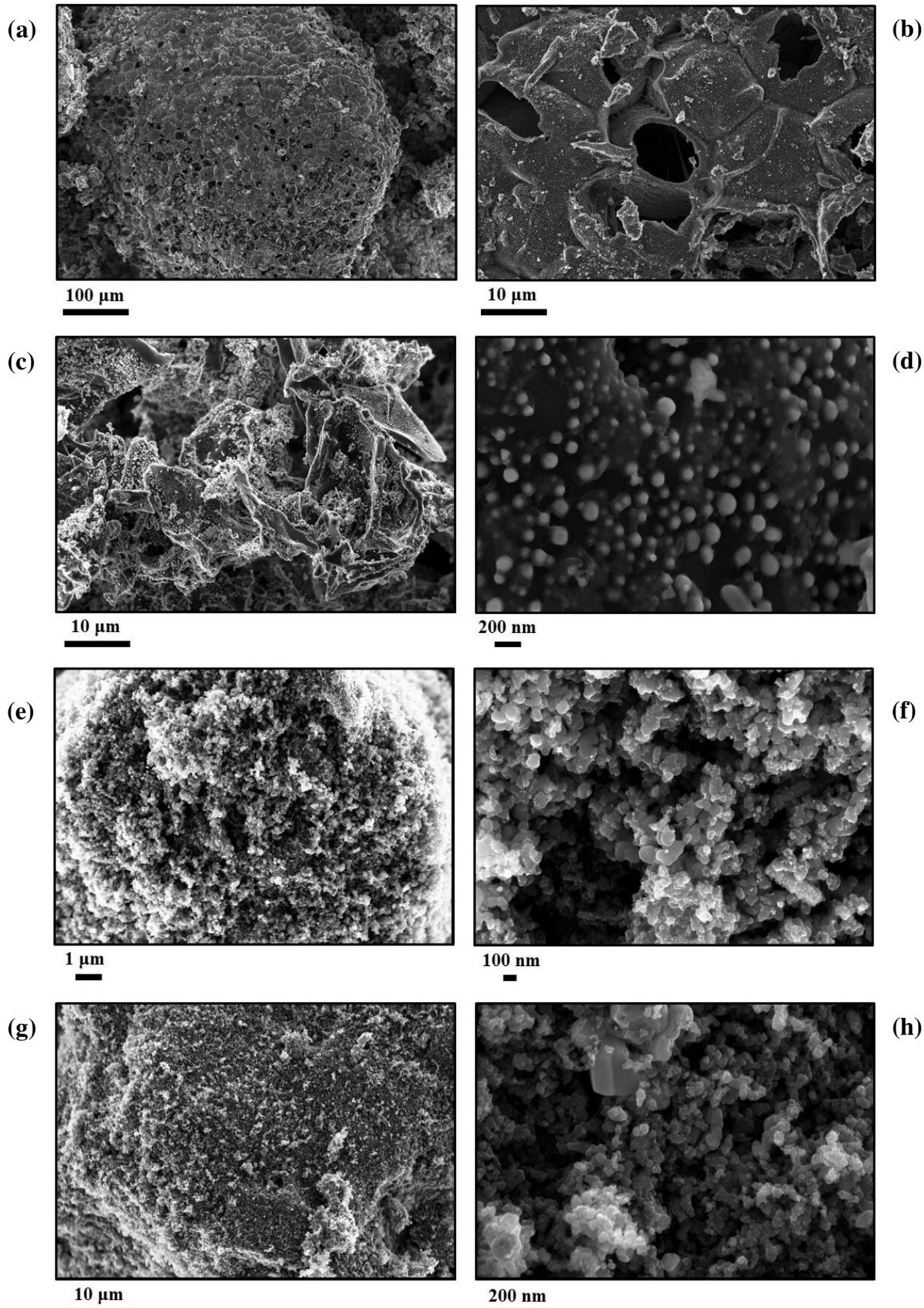

Fig. 2. FESEM captions of a-b) biochar from exhausted coffee, c-d) CC prior catalysis, e-f) carbonized tires and g-h) TC prior catalysis.

synthesis of catalysts [43,44]. This facile approach has been used to tailor the surface of carbon from pyrolysis of exhausted coffee and waste tires with metal nanostructures as those shown in Fig. 2.

The surface of the coffee biochar prior carbothermal process (Fig. 2 a-b) was structured in micrometric sponge-like aggregates whose diameter is around 20 to 100 µm. Coffee biochar shows a very low specific surface area of up to 0.14 m^2/g manly due to the presence of micrometric pores formed during the release of volatile organic matters from the inner core of biomass particles. Contrary, carbon recovered from pyrolysis of tires showed a structure closely related to carbon black used for tires production [45]. This material was composed by of a complex agglomeration of carbon nanoparticles (similar to carbon black structure) with a specific surface area of up 37.7 m^2/g. Carbothermal synthesis of CC induces the formation on the carbonaceous surface of semispherical iron particles with diameters ranging from 50 to 150 nm (Fig. 2 c-d). CC surface area increased of up to 46.2 m^2/g due to the

Table 1
Elementary composition of pyrolyzed waste coffee obtained through EDX analysis, I_D/I_G and surface area before and after deposition of Fe nanoparticles.

	Elemental analysis (wt%)											I_D/I_G	Surface area (m^2/g)
	C	O	Mg	P	K	Ca	Fe	Si	S	Zn	Na		
Coffee biochar	86.9	8.9	0.6	0.5	1.8	1.3	Not detected	Not detected	Not detected	Not detected	Not detected	2.13	0.1
TC	70.9	7.8	Not detected	Not detected	Not detected	1.5	19.8	0.5	1.3	1.5	Not detected	2.72[b]	53.9
TC[a]	72.8	4.4	Not detected	Not detected	Not detected	Not detected	21.1	0.2	0.5	Not detected	Not detected		52.1
CC	62.2	11.6	0.6	0.3	3.5	0.7	21.2	Not detected	Not detected	Not detected	Not detected	2.04[b]	46.2
CC[a]	60.5	15.8	0.7	1.1	1.2	0.7	19.5	Not detected	Not detected	Not detected	0.5		44.9

a) Catalysts after third catalytic cycle, b) I_D/I_G was unchanged before and after third catalytic cycle since the Raman spectra did not show any appreciable differences.

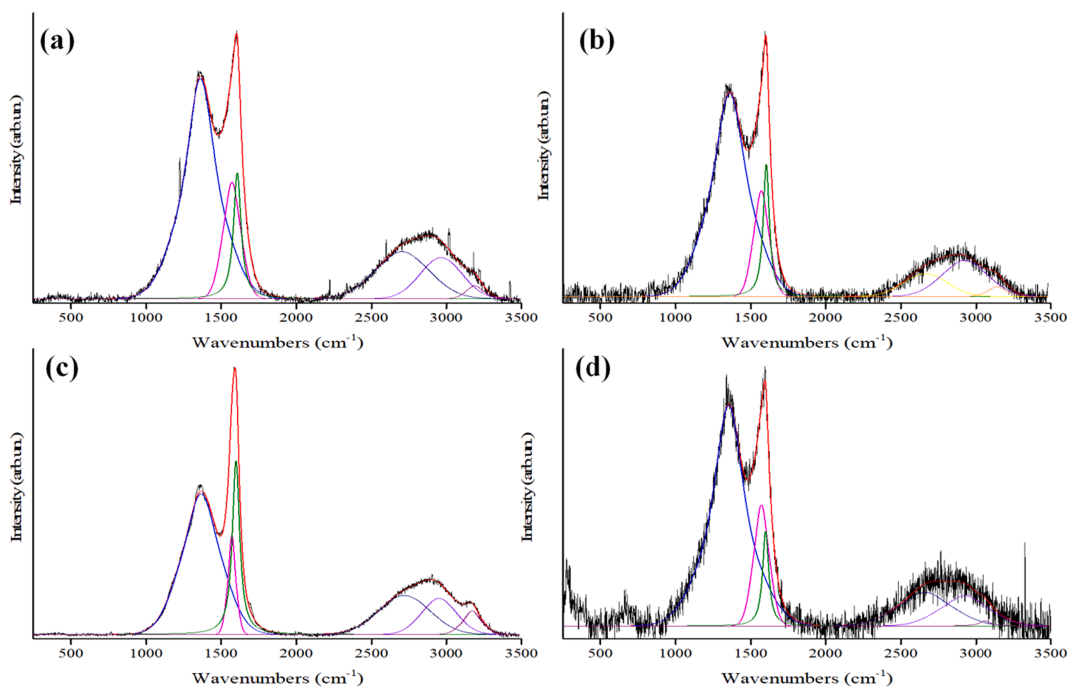

Fig. 3. Raman spectra of a) biochar from exhausted coffee a coffee, b) CC prior catalysis, c) carbonized tires and d) TC prior catalysis. In black was reported the original Raman spectra and in red the fitted ones accordingly with the procedure proposed by Tagliaferro et al [42]. (For interpretation of the references to colour in this figure legend, the reader is referred to the web version of this article.)

presence of nanoparticles together with the activation of carbon matrix, as described by Wang et al. [46]. Similarly, TC displayed spherical iron nanoparticles anchored to carbon together with submicrometric iron aggregate (Fig. 2 h). TC showed a specific surface area increment of up to 53.9 m^2/g mainly ascribed in this case to the presence of iron species. The more Comparing structures reported in Fig. 2d and Fig. 2 h, we observed that iron nanoparticles are fully exposed on surface of CC due the bigger size of carbon support compared with growing iron nanoparticles. Considering TC, carbon black particles were much smaller compared with iron nanoparticles and were unable to provide an anchoring surface as in the case of CC partially covering the nanostructures formed.

The elementary compositions of the CC, TC and their precursors were estimated by using EDX analysis as shown in Table 1.

Coffee biochar showed an amount of carbon as carbon recovered from tires together with an appreciable amount of oxygen that could be associated to both residual group on carbon surface and to inorganic species. Inorganic species in coffee derived biochar derived from the biological fixation routes that originates the feedstock [47]. Additionally, carbon recovered from tires displayed a sulphur content of up to 0.5 wt% due to the not complete conversion of sulphur into organic or volatile organic matters as previously described by Undri et al. [48]. Furthermore, TC precursors showed a negligible native iron content estimated in less than 0.1 wt% by analysis its ash content. After, carbothermal process TC showed a totally disappearing of sulphur due to its oxidation with formation of SO_x. The final [Fe] was attested in both cases around to 20 wt% (19.8 wt% and 21.2 wt% for TC and CC respectively).

A further investigation of carbon structure of CC, TC and their precursors was run by using Raman spectroscopy as reported in Fig. 3.

Raman spectroscopy is a powerfully tool to estimate the carbon degree of graphitization [49]. Particularly, the area ratio of D and G peaks in the region from 1300 to 1700 cm^{-1} (I_D/I_G) is possible investigated the carbonaceous structure disorder. Both coffee derived biochar and carbon recovered from waste tires were highly disordered materials with a I_D/I_G of up to 2.13 and 2.04 respectively [50]. After carbothermal process, CC and TC showed a decrement of I_D/I_G down to 2.04 while TC showed an increment of up to 2.72. This different behavior could be ascribed to the intrinsically differences between the two precursors. CC was produced by using a material that retained a relevant amount of

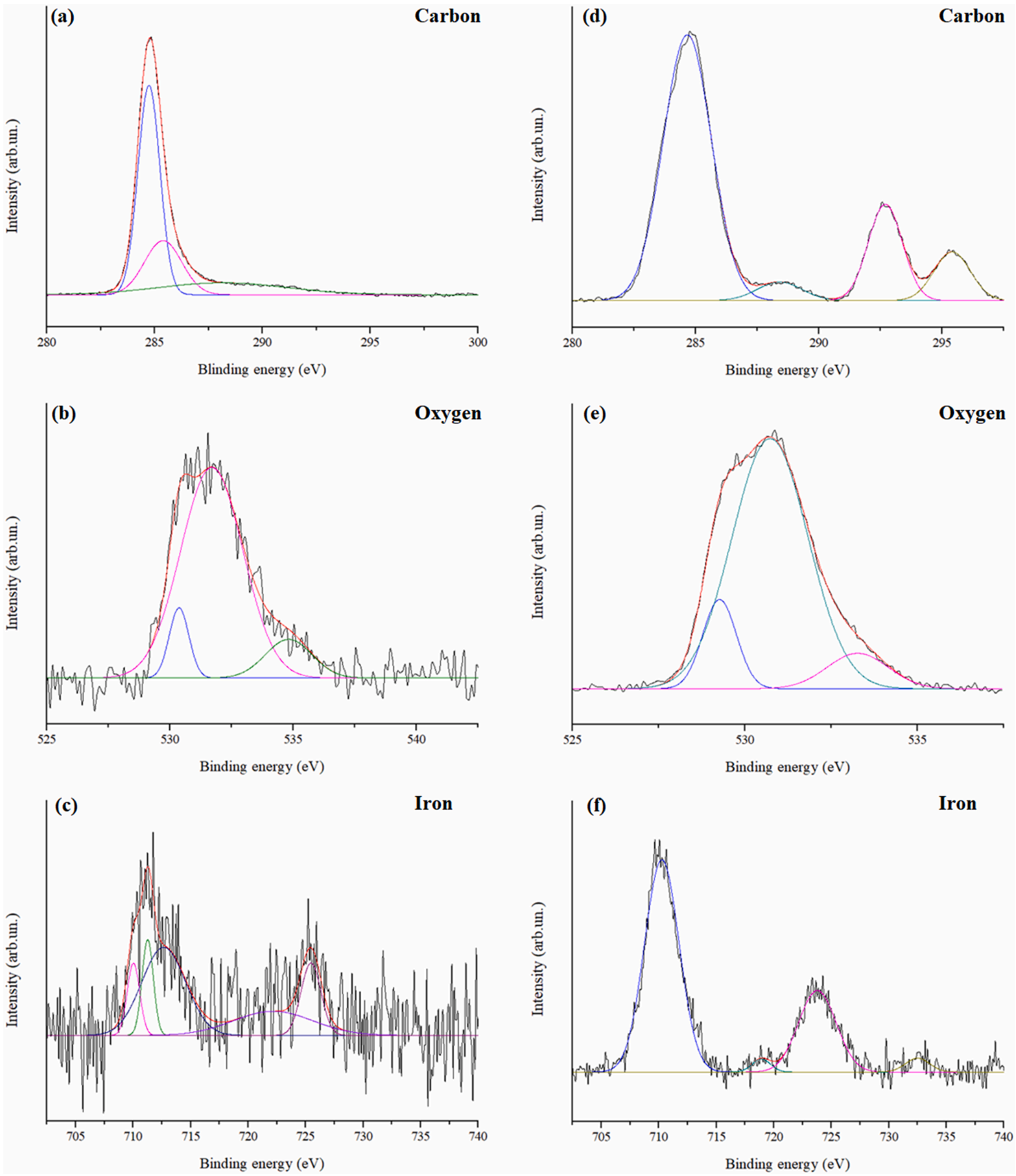

Fig. 4. XPS spectra of CC (a-c) and TC (d-f). Carbon, oxygen and iron region are here displayed.

residual functional groups and sp^3 carbon content while carbon recovered from carbonization of tires was mainly composed by original carbon used to produce the neat tires. Considering CC, carbothermal process polished partially the carbon surface with a decrement of imperfections of carbonaceous structure while those are magnified for TC that was more ordered. This was also confirmed by the analysis of XPS spectra reported in the Fig. 4.

XPS spectra of CC (Fig. 4 a) showed a high amount of sp^2 carbon preponderance (peak 284 eV) that reach the 68.5% of the total amount while sp^3 represented only the 17.5% (peak 284.9 eV). TC was composed by only sp^2 carbon that was highly functionalized by oxygen functionalities proving the disorder observed by Raman spectroscopy. Those oxygen functionalities displayed peaks at 529, 531 and 533 eV. Peak at 531 eV represented up to 79% for both CC and TC and it was associated with the presence of oxygen linked to quinoid carbons. The peak at 529.3 eV with a relative area of around 12% was instead attributed to an oxygen bound to an iron in iron oxide [51]. Furthermore, the presence of Fe-OH residue on the particle surface was proved by the peak at 533.3 eV that represent the 8.9% of the total area

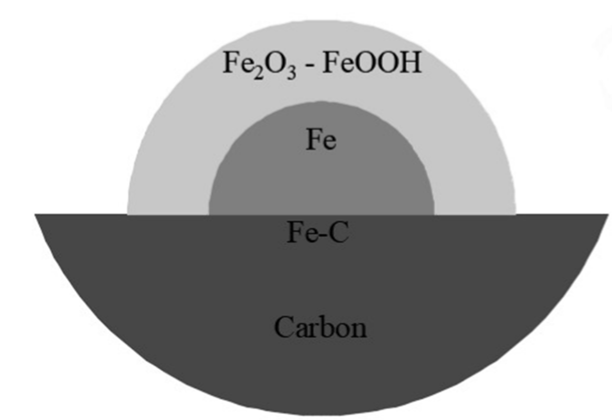

Fig. 5. Hypothesized structure of iron particles anchored onto carbon support after carbothermal reduction and air passivation.

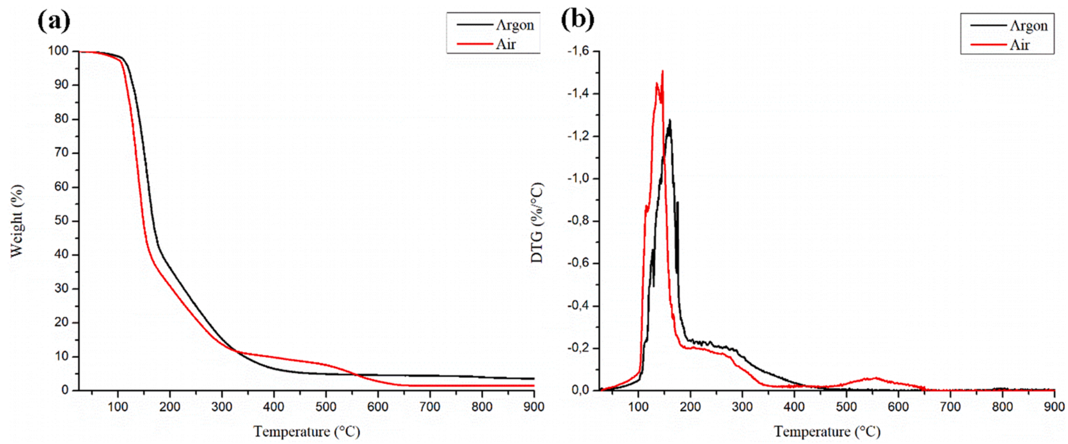

Fig. 6. TGA and DTG of tire oil at Ar and air atmosphere from 25 °C to 900 °C.

Table 2
Catalytic performances of CC and TC during oxidative desulphurization of high sulphur content oil recovered from pyrolysis of tires.

Entry	Catalyst	T (°C)	T (h)	Desulphurization[(a)] (%)	[S] (ppm)	Loading[(b)] (wt%)/TON[(c)]
1	–	100	6	33.2	4769	–
2	CC	100	2	47.5	3747	5/219
3		100	4	52.3	3406	5/241
4		100	6	63.7	2592	5/293
5		60	6	36.4	4540	5/168
6		80	6	52.0	3425	5/240
7		100	6	49.0	3639	2/565
8		100	6	40.8	4223	10/94
9		100[(d)]	6	39.2	3747	5/181
10	TC	100	2	57.5	3036	5/283
11		100	4	58.1	2989	5/286
12		100	6	56.1	3132	5/276
13		60	6	34.0	4709	5/167
14		80	6	36.1	4564	5/177
15		100	6	53.7	3305	2/660
16		100	6	52.2	3415	10/128
17		100[(d)]	6	42.3	4116	5/169

(a) Desulphurization = 100-(100*final sulphur concetration/initial sulphur concentration), (b) loading = 100* (weight of iron/weight of oil), [(c)]TON = mmol of removed sulphur/mmol of accessible iron sites [(d)]3rd cycle of desulphurization.

[52]. The small area underlying this last peak shows that these groups exist only on the surface of the Fe nanoparticle and render the metal oxide layer partially defective. The formation of this defects could be ascribed to the presence of FeOOH formed during air passivation of iron nanoparticles as reported by Ponder et al. [53] at room temperature [54]. Accordingly to Fig. 4 c and f, the spectrum of iron was shown and the presence of metallic iron and iron oxide across the peaks at 710.5 and 712.2 eV was detected. Iron oxidation state was in agreement with the peak at 530.0 eV of the oxygen spectrum, typical of a metal oxide. From the conclusions extrapolated from the carbon characterization before and after the carbothermic process, it was possible to obtain a model of the iron nanoparticle supported on a carbonaceous matrix. As can be seen from Fig. 5, the hypothesized iron nanoparticle model was based on a metallic iron core whose external surface was made by a layer of Fe_2O_3 and FeOOH sites generated through passivation attached to the surface of the pyrolytic carbon through a very thin layer of iron carbide accordingly to Li et al. [55]. CC showed a Fe(III)/Fe(0) ratio of 55.7% while TC showed a value of 53.3%.

3.2. Preliminary considerations about oil recovered from pyrolysis of waste tires

Pyrolysis of waste tires was run at 550 °C accordingly with Ucar et al. [56] trying to maximizing the liquid yield. Nonetheless, the temperature adopted promoted the highest polycyclic sulphur aromatic compounds content as reported by Williams et al. [57]. In our study, oil recovered from the exhausted tires pyrolysis showed a concentration of up to 7139 ppm that greatly exceed the limit for use as drop-in fuel. Nonetheless, the TGA profiles of oil shown in Fig. 6 confirmed a composition close to a conventional fuel, rich in C_6-C_{10} hydrocarbons, accordingly with the study reported by Kök et al. [58].

Furthermore, the weigh losses between 500 °C and 600 °C could be attributed to the presence of polycyclic aromatic hydrocarbons which are more resistant to oxidation than other hydrocarbons.

3.3. Catalytic activity of CC and TC in oxidative desulphurization of oil recovered from pyrolysis of waste tires

Catalytic oxidative desulphurization of high sulphur content oil recovered from pyrolysis of tires was study by using CC and TC and varying several parameters as shown in table 2.

Comparing the removal efficiencies of the catalysts and the H_2O_2 (desulphurization of up to 33.2) under the same operating conditions (6 h at 100° C with 5% g Fe / g oil) was evident the improvement induced by CC and TC that reached a desulphurization of up to 63.7% and 53.7%. CC displayed the better performances compared with TC according to TON values. This was reasonably due to the effect of different carbon matrix. CC present iron nanoparticles fully exposed on the surface while TC was characterized by iron particles surrounded by nanometric carbon particles. Accordingly, TC activity could deplete by the hindrance of

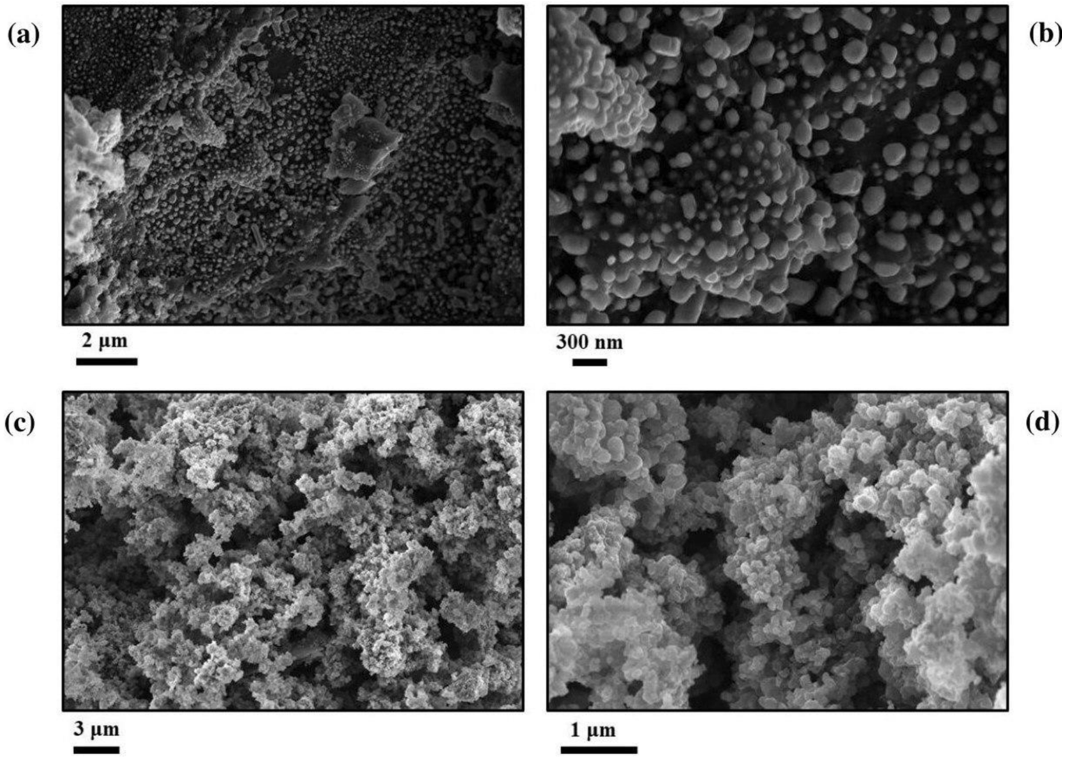

Fig. 7. FESEM captions at different magnifications of CC (a-b) and TC (c-d) after three catalytic cycles.

carbon matrix with lower iron nanoparticles accessibility.

By examining the entries 12, 13 and 14, an improvement in sulfur removal at high temperatures can be seen due to an evident kinetic boost. TC desulphurization rose from 36.1% at 80 °C of up to 56.1% at 100 °C. Similarly, temperature improved the CC desulphurization activity from 36.4% to 63.7% of. Temperature effect was scarcely influenced by the support but it was more related the activation energy together with phase transfer equilibria [59].

The catalyst loading is the other key parameter of the investigated. Catalyst loading of 2% induced a reduction of desulphurization compared to the use of 5% for both CC and TC. Surprisingly, a catalyst loading of up to 10 wt% lead to a decrement of desulphurization at 100 °C after 6 h down to 40.8% for CC while TC was unaffected. This was reasonably due to aggregation phenomena of micrometric particles of CC that did not occurred by using TC composed by nanometric carbon particles. Additionally, the original high sulphur content represented an obstacle to an efficient removal by using a biphasic approach with the extracted sulphone that rapidly reached the saturation of watery phase. Nonetheless, CC and TC displayed catalytic performances very close to systems operating on tires derived oil [28,60] even if none of previously published research based on biphasic systems treated oil with a sulphur content high such the one used in the present study.

Both CC and TC showed a reduction of activity after the third catalytic cycle down to 39.2% and 42.3% respectively. This was not related to iron leaching as proved by iron content retention as shown in table 2 but it was ascribed by a sized increment of iron particles as shown in Fig. 7.

CC showed an increment of particles average diameter of up to 100–300 nm while TC shows iron aggregated covered by spherical carbon nanoparticles.

However, the XPS spectra of recycled catalysts (Fig. 8) support the observed loss of reactivity due to the composition change on the catalyst surface.

The loss of reactivity was also due to the increasing of the thickening of the crystal lattice of the iron oxide which reduces the tension on the same thus relaxing the orbitals. About each spectrum shown in Fig. 8, the iron signal of TC (Fig. 8 f) was characterized by a high noise level which did not allow the detection of any peak. A fitting analysis of the iron spectrum of CC was performed although the large noise because of the micrometric size of the unpacked material from this type of catalyst. In particular, five peaks were distinct (the last two are replicas) while the three initial peaks are identifiable to a metallic iron, Fe-OH and iron oxide. About oxygen spectra, the position of the oxygen peaks has remained unchanged, so the catalyst continues to present oxides of iron and oxygen of a quinoidic nature. While the signal of carbon (Fig. 8 a), the spectrum of CC a showed the insertion of a new peak at 285.3 eV which is associated with the formation of a C-OH bond caused by the action of H_2O_2. The other two peaks at 284 and 288.1 eV of area, respectively, of 56.8 and 18.9% of the total, mark, as previously seen, the presence of C sp^2 and C of a quinoidic nature.

We supposed that the original structures of CC and TC underwent to different deactivation process as such reported in Fig. 9

According with FESEM analysis (Fig. 8 b), iron nanoparticles anchored onto CC increased their sized with a decrement of available catalytic sites on the surface. TC deactivation was mainly due to the covering of the iron nanoparticles by the spherical carbon particles of the support. This proved lower anchoring of iron nanostructures to TC than CC. The surface flattering of CC was caused by the unpacking of micrometric carbon particles so modifying the surface morphology, as shown in Fig. 7 a.

4. Conclusions

In this work we reported the production and catalytic desulphurization of high sulphur content oil recovered from pyrolysis of tires by using biphasic catalytic oxidative desulphurization. Catalytic systems proposed were based on conversion of two waste streams through a facile carbothermal process capable to produce highly active heterogeneous catalysts characterized by nanostructured iron-based material. Air passivation after the carbothermal processes was a key step for

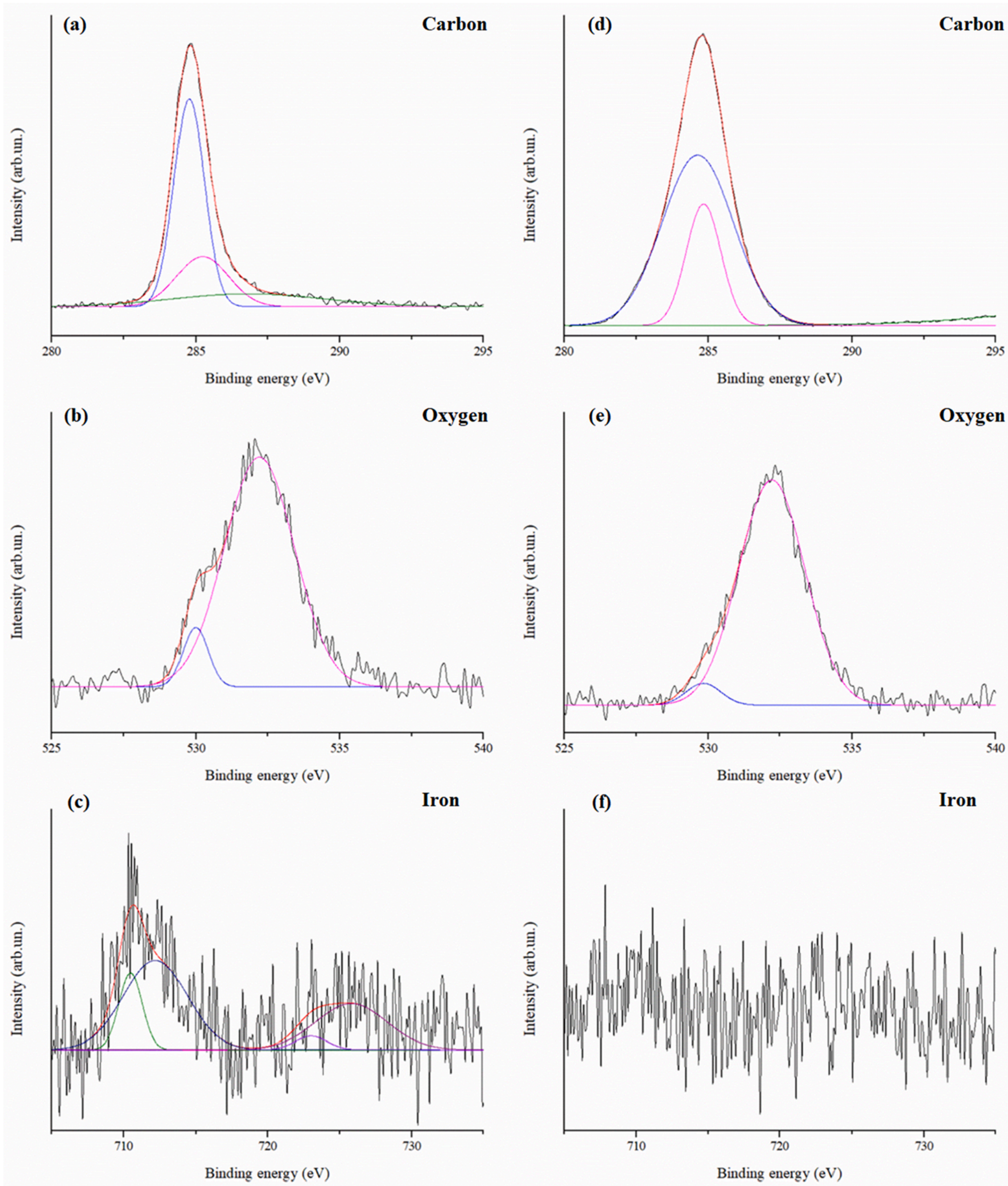

Fig. 8. XPS spectra of CC (a-c) and TC (d-f) after the 3rd catalytic run. Carbon, oxygen and iron region are here displayed.

achieving a hemispherical external layer of Fe_2O_3 and FeOOH on an iron-based core. Thanks to the special geometry of the catalytic system created, CC showed a desulphurization ability of up to over 60% by using high sulphur content oil at the best conditions (at 100 °C with a residence time of 6 h). The morphological characteristics of the pyrolyzed waste streams were fundamental to describe the behavior of the catalytic system during the desulfurization processes. TC was successful in maintaining constant the desulphurization rate at different conditions thanks to submicrometric structure which increases the phase transfer between the reactants in the biphasic system. While the CC shows a micrometric structure, covered by nanometric iron-based particles, which tends to influence more the kinetics of the catalytic system. Despite this, iron-based materials produced by carbothermic processes could be considered a great improvement in Fenton reactions for oxidative desulphurization thanks to easier separation through magnetic proprieties and absence of leaching into reaction solution.

CRediT authorship contribution statement

Valentina Tamborrino: Validation, Formal analysis, Data curation, Writing - original draft, Visualization. **Giulia Costamagna:** Validation, Formal analysis, Data curation. **Mattia Bartoli:** Validation, Formal analysis, Investigation, Data curation, Writing - original draft, Writing - review & editing, Supervision. **Massimo Rovere:** Validation, Formal analysis, Data curation, Writing - review & editing. **Pravin Jagdale:** Formal analysis, Investigation, Data curation, Writing - review & editing. **Luca Lavagna:** Formal analysis, Data curation, Writing - review & editing. **Marco Ginepro:** Validation, Investigation, Resources, Data curation, Writing - review & editing. **Alberto Tagliaferro:** Validation, Investigation, Resources, Data curation, Writing - review & editing, Supervision.

Declaration of Competing Interest

The authors declare that they have no known competing financial

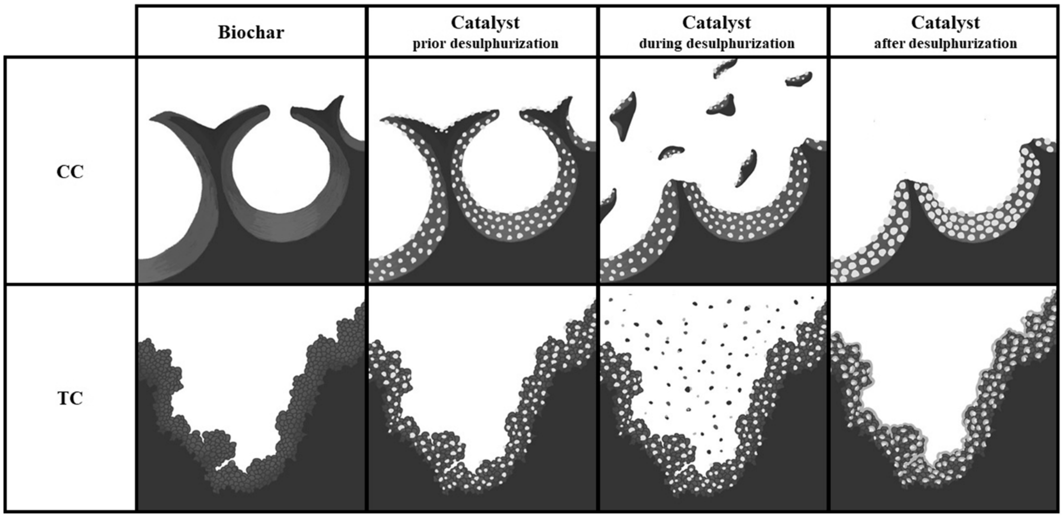

Fig. 9. Evolution of the catalysts during the catalytic oxidative desulphurization of oil from tires pyrolysis.

interests or personal relationships that could have appeared to influence the work reported in this paper.

References

[1] Leiserowitz AA, Kates RW, Parris TM. Sustainability values, attitudes, and behaviors: a review of multinational and global trends. Annu Rev Environ Resour 2006;31(1):413–44.
[2] Nadal M, Rovira J, Díaz-Ferrero J, Schuhmacher M, Domingo JL. Human exposure to environmental pollutants after a tire landfill fire in Spain: health risks. Environ Int 2016;97:37–44.
[3] Singh A, Spak SN, Stone EA, Downard J, Bullard RL, Pooley M, et al. Uncontrolled combustion of shredded tires in a landfill–Part 2: population exposure, public health response, and an air quality index for urban fires. Atmos Environ 2015;104: 273–83.
[4] Lavagna L, Nisticò R, Sarasso M, Pavese M. An analytical mini-review on the compression strength of rubberized concrete as a function of the amount of recycled tires crumb rubber. Materials 2020;13(5):1234.
[5] Záleská M, Pavlík Z, Čítek D, Jankovský O, Pavlíková M. Eco-friendly concrete with scrap-tyre-rubber-based aggregate–properties and thermal stability. Constr Build Mater 2019;225:709–22.
[6] Gupta T, Siddique S, Sharma RK, Chaudhary S. Behaviour of waste rubber powder and hybrid rubber concrete in aggressive environment. Constr Build Mater 2019; 217:283–91.
[7] Lo Presti D. Recycled tyre rubber modified Bitumens for road asphalt mixtures: a literature review. Constr Build Mater 2013;49:863–81.
[8] Quadrini F, Santo L, Musacchi E. A sustainable molding process for new rubber products from tire recycling. Prog Rubber Plast Recycl Technol 2019;35(1):41–55.
[9] Schmidt M, Spieth H, Haubach C, Kühne C. Rubber mats made from recycled used tyres. In: 100 pioneers in efficient resource management. Springer; 2019. p. 222–5.
[10] Sunthonpagasit N, Duffey MR. Scrap tires to crumb rubber: feasibility analysis for processing facilities. Resour Conserv Recycl 2004;40(4):281–99.
[11] Banaszkiewicz K, Badura M. Experimental investigation on the application of recycled tires polymer fibers as a BTEX removal material. SN Appl Sci 2019;1(6): 558.
[12] Labaki M, Jeguirim M. Thermochemical conversion of waste tyres—a review. Environ Sci Pollut Res 2017;24(11):9962–92.
[13] Martínez JD, Puy N, Murillo R, García T, Navarro MV, Mastral AM. Waste tyre pyrolysis–a review. Renew Sustain Energy Rev 2013;23:179–213.
[14] Sathiskumar C, Karthikeyan S. Recycling of waste tires and its energy storage application of by-products–a review. Sustainable Mater Technol 2019;22. e00125.
[15] Kyari M, Cunliffe A, Williams PT. Characterization of oils, gases, and char in relation to the pyrolysis of different brands of scrap automotive tires. Energy Fuels 2005;19(3):1165–73.
[16] Rajendran A, Cui T-Y, Fan H-X, Yang Z-F, Feng J, Li W-Y. A comprehensive review on oxidative desulfurization catalysts targeting clean energy and environment. J Mater Chem A 2020;8(5):2246–85.
[17] Iruretagoyena D, Montesano R. Selective sulfur removal from liquid fuels using nanostructured adsorbents. In: Nanotechnology in oil and gas industries. Springer; 2018. p. 133–50.
[18] Anastas P, Eghbali N. Green chemistry: principles and practice. Chem Soc Rev 2010;39(1):301–12.
[19] Murata S, Murata K, Kidena K, Nomura M. A novel oxidative desulfurization system for diesel fuels with molecular oxygen in the presence of cobalt catalysts and aldehydes. Energy Fuels 2004;18(1):116–21.
[20] Yan X-M, Mei P, Lei J, Mi Y, Xiong L, Guo L. Synthesis and characterization of mesoporous phosphotungstic acid/TiO2 nanocomposite as a novel oxidative desulfurization catalyst. J Mol Catal A: Chem 2009;304(1):52–7.
[21] Sampanthar JT, Xiao H, Dou J, Nah TY, Rong Xu, Kwan WP. A novel oxidative desulfurization process to remove refractory sulfur compounds from diesel fuel. Appl Catal B 2006;63(1-2):85–93.
[22] Trakarnpruk W, Rujiraworawut K. Oxidative desulfurization of gas oil by polyoxometalates catalysts. Fuel Process Technol 2009;90(3):411–4.
[23] Lü H, Gao J, Jiang Z, Yang Y, Song Bo, Li C. Oxidative desulfurization of dibenzothiophene with molecular oxygen using emulsion catalysis. Chem Commun 2007;(2):150–2. https://doi.org/10.1039/B610504A.
[24] Zhang W, Zhang H, Xiao J, Zhao Z, Yu M, Li Z. Carbon nanotube catalysts for oxidative desulfurization of a model diesel fuel using molecular oxygen. Green Chem 2014;16(1):211–20.
[25] Collins FM, Lucy AR, Sharp C. Oxidative desulphurisation of oils via hydrogen peroxide and heteropolyanion catalysis. J Mol Catal A: Chem 1997;117(1-3): 397–403.
[26] Wang D, Qian EW, Amano H, Okata K, Ishihara A, Kabe T. Oxidative desulfurization of fuel oil: Part I. Oxidation of dibenzothiophenes using tert-butyl hydroperoxide. Appl Catal A 2003;253(1):91–9.
[27] Zhu W, Li H, Gu Q, Wu P, Zhu G, Yan Y, et al. Kinetics and mechanism for oxidative desulfurization of fuels catalyzed by peroxo-molybdenum amino acid complexes in water-immiscible ionic liquids. J Mol Catal A: Chem 2011;336(1-2):16–22.
[28] Haw K-G, Bakar WAWA, Ali R, Chong J-F, Kadir AAA. Catalytic oxidative desulfurization of diesel utilizing hydrogen peroxide and functionalized-activated carbon in a biphasic diesel–acetonitrile system. Fuel Process Technol 2010;91(9): 1105–12.
[29] Zhang M, Zhu W, Xun S, Li H, Gu Q, Zhao Z, et al. Deep oxidative desulfurization of dibenzothiophene with POM-based hybrid materials in ionic liquids. Chem Eng J 2013;220:328–36.
[30] Li C, Jiang Z, Gao J, Yang Y, Wang S, Tian F, et al. Ultra-deep desulfurization of diesel: oxidation with a recoverable catalyst assembled in emulsion. Chem-Eur J 2004;10(9):2277–80.
[31] Zhang Q, Zhu M, Jones I, Zhang Z, Zhang D. Desulfurization of spent tire pyrolysis oil and its distillate via combined catalytic oxidation using H2O2 with formic acid and selective adsorption over Al2O3. Energy Fuels 2020;34(5):6209–19.
[32] Neyens E, Baeyens J. A review of classic Fenton's peroxidation as an advanced oxidation technique. J Hazard Mater 2003;98(1-3):33–50.
[33] Barb WG, Baxendale JH, George P, Hargrave KR. Reactions of ferrous and ferric ions with hydrogen peroxide. Nature 1949;163(4148):692–4.
[34] Zhang J, Wang G, Zhang L, Fu X, Liu Y. Catalytic oxidative desulfurization of benzothiophene with hydrogen peroxide catalyzed by Fenton-like catalysts. Reaction Kinetics, Mech Catal 2014;113(2):347–60.
[35] Flores R, Rodas A, Gasperin R. Oxidative desulfurization of diesel fuel oil using supported Fenton catalysts and assisted with ultrasonic energy. Pet Sci 2019;16(5): 1176–84.
[36] Shen Y. Carbothermal synthesis of metal-functionalized nanostructures for energy and environmental applications. J Mater Chem A 2015;3(25):13114–88.
[37] Hoch LB, Mack EJ, Hydutsky BW, Hershman JM, Skluzacek JM, Mallouk TE. Carbothermal synthesis of carbon-supported nanoscale zero-valent iron particles for the remediation of hexavalent chromium. Environ Sci Technol 2008;42(7): 2600–5.
[38] Arrigo R, Bartoli M, Malucelli G. Poly (lactic acid)–biochar biocomposites: effect of processing and filler content on rheological, thermal, and mechanical properties. Polymers 2020;12(4):892.
[39] Arrigo R, Jagdale P, Bartoli M, Tagliaferro A, Malucelli G. Structure-property relationships in polyethylene-based composites filled with biochar derived from waste coffee grounds. Polymers 2019;11(8):13.

[40] Giorcelli M, Bartoli M. Development of coffee biochar filler for the production of electrical conductive reinforced plastic. Polymers 2019;11(12):17.

[41] Strongone V, Bartoli M, Jagdale P, Arrigo R, Tagliaferro A, Malucelli G. Preparation and characterization of UV-LED curable acrylic films containing biochar and/or multiwalled carbon nanotubes: effect of the filler loading on the rheological, thermal and optical properties. Polymers 2020;12(4):796.

[42] Tagliaferro A, Rovere M, Padovano E, Bartoli M, Giorcelli M. Introducing the novel mixed gaussian-lorentzian lineshape in the analysis of the raman signal of biochar. Nanomaterials 2020;10(9):1748.

[43] Thompson E, Danks AE, Bourgeois L, Schnepp Z. Iron-catalyzed graphitization of biomass. Green Chem 2015;17(1):551–6.

[44] Bartoli M, Giorcelli M, Jagdale P, Rovere M, Tagliaferro A. A review of non-soil biochar applications. Materials 2020;13(2):291–6.

[45] Gómez-Hernández R, Panecatl-Bernal Y, Méndez-Rojas MÁ. High yield and simple one-step production of carbon black nanoparticles from waste tires. Heliyon 2019;5(7). e02139.

[46] Wang Y, Xia Q, Bai X, Ge Z, Yang Q, Yin C, et al. Carbothermal activation synthesis of 3D porous g-C3N4/carbon nanosheets composite with superior performance for CO2 photoreduction. Appl Catal B 2018;239:196–203.

[47] Grembecka M, Malinowska E, Szefer P. Differentiation of market coffee and its infusions in view of their mineral composition. Sci Total Environ 2007;383(1-3):59–69.

[48] Undri A, Sacchi B, Cantisani E, Toccafondi N, Rosi L, Frediani M, et al. Carbon from microwave assisted pyrolysis of waste tires. J Anal Appl Pyrol 2013;104:396–404.

[49] Ferrari AC, Robertson J. Interpretation of Raman spectra of disordered and amorphous carbon. Phys Rev B 2000;61(20):14095–107.

[50] Guizani C, Haddad K, Limousy L, Jeguirim M. New insights on the structural evolution of biomass char upon pyrolysis as revealed by the Raman spectroscopy and elemental analysis. Carbon 2017;119:519–21.

[51] Yamashita T, Hayes P. Analysis of XPS spectra of Fe2+ and Fe3+ ions in oxide materials. Appl Surf Sci 2008;254(8):2441–9.

[52] McIntyre NS, Zetaruk DG, Owen D. X-Ray photoelectron studies of the aqueous oxidation of Inconel-600 alloy. J Electrochem Soc 1979;126(5):750–60.

[53] Ponder SM, Darab JG, Bucher J, Caulder D, Craig I, Davis L, et al. Surface chemistry and electrochemistry of supported zerovalent iron nanoparticles in the remediation of aqueous metal contaminants. Chem Mater 2001;13(2):479–86.

[54] Fung KK, Qin B, Zhang XX. Passivation of α-Fe nanoparticle by epitaxial γ-Fe2O3 shell. Mater Sci Eng, A 2000;286(1):135–8.

[55] Li J, Lan H, Liu H, Zhang G, An X, Liu R, et al. Intercalation of nanosized Fe3C in iron/carbon to construct multifunctional interface with reduction, catalysis, corrosion resistance, and immobilization capabilities. ACS Appl Mater Interfaces 2019;11(17):15709–17.

[56] Ucar S, Karagoz S, Ozkan AR, Yanik J. Evaluation of two different scrap tires as hydrocarbon source by pyrolysis. Fuel 2005;84(14-15):1884–92.

[57] Williams PT, Bottrill RP. Sulfur-polycyclic aromatic hydrocarbons in tyre pyrolysis oil. Fuel 1995;74(5):736–42.

[58] Kök MV, Varfolomeev MA, Nurgaliev DK. Crude oil characterization using TGA-DTA, TGA-FTIR and TGA-MS techniques. J Petrol Sci Eng 2017;154:537–42.

[59] García-Gutiérrez JL, Fuentes GA, Hernández-Terán ME, García P, Murrieta-Guevara F, Jiménez-Cruz F. Ultra-deep oxidative desulfurization of diesel fuel by the Mo/Al2O3-H2O2 system: The effect of system parameters on catalytic activity. Appl Catal A 2008;334(1-2):366–73.

[60] Hossain MN, Choi MK, Park HC, Choi HS. Purifying of waste tire pyrolysis oil using an S-ZrO2/SBA-15-H2O2 catalytic oxidation method. Catalysts 2020;10(4):368.